# One-dimensional transport with dynamic disorder

Valeri Barsegov,[1] Yonathan Shapir,[2] and Shaul Mukamel[1,2]
[1]*Department of Chemistry, University of Rochester, Rochester, New York 14627-0216, USA*
[2]*Department of Physics and Astronomy, University of Rochester, Rochester, New York 14627-0216, USA*
(Received 7 March 2003; published 11 July 2003)

We study the mean quenching time distribution and its moments in a one-dimensional $N$-site donor-bridge-acceptor system where all sites are coupled to a two-state jump bath for arbitrary disorder and an arbitrary ratio $\kappa \equiv \langle k \rangle / R$ of the bath jump rate $R$ and the average hopping rate $\langle k \rangle$. When $\kappa N \sim 1$, the quenching time distribution has long power-law tails even when the waiting times are exponentially distributed. These disappear for $\kappa N \ll 1$ where the hopping rate self-averages on the bath relaxation time scale. In the absence of disorder or for small $\kappa$, the mean quenching time scales linearly with $N$. Otherwise, we observe a power law, $\sim N^{1+\gamma}$, with a crossover to linear scaling ($\gamma = 0$) for large $N$. Distributions of particle position, its second moment, velocity and diffusion coefficient are computed in the infinite $N$ limit. For times longer than $R^{-1}$, the dynamic disorder self-averages and the average position, velocity, and diffusion coefficient scale linearly in time.

DOI: 10.1103/PhysRevE.68.011101 PACS number(s): 05.40.Fb, 82.37.−j, 72.20.Ee

## I. INTRODUCTION

Disordered systems are usually divided into two classes depending on whether the disorder is annealed (dynamic) or quenched (static) [1–4]. This paper studies the scaling properties of one-dimensional directed walk [5–7] with dynamic disorder. Models of directed walk have been used to analyze numerous systems, including excitation transport from a donor chromophore through a bridge of intermediate sites to an acceptor where this excitation is quenched [8–12], lateral diffusion of proteins on the surface of a membrane [13–15], charge transport in single molecular wires and DNA [16–18], diffusion in ion channels [19–24], and polymer translocation through a narrow pore [25–29].

The effects of fluctuating environment on transport are of considerable interest [30–36]. When $\kappa N \ll 1$, where $N$ is the total number of sites, $\kappa \equiv \langle k \rangle / R$, $R$ is the bath jump rate, and $\langle k \rangle$ is the average hopping rate, transport is unaffected by environment fluctuations. However, this is not the case in the presence of dynamic disorder, i.e., when transport and bath jumps are coupled and occur on a compatible time scale. This is an important regime relevant to many biophysical systems. For example, excitation transfer may occur while the bridge conformation fluctuates spanning a manifold of conformational states. Some of these states may facilitate fast transport whereas in others the excitation may be trapped [35,37]. Protein rare jumps over or through the cytoskeletal fence between ''corralled regions'' in membranes may take place over the same time scale as the reorganization of the matrix itself [13]. Matrix fluctuations can either open or close the gate of a ''skeleton fence'' and thus, may affect protein transport. Charge transfer from donor to an acceptor can occur while a molecule undergoes vibrational energy redistribution which may alter the donor and acceptor wave function overlap and thereby affect conductance. Ion diffusion may occur at comparable time as geometry fluctuation of a channel [19–23], which may increase or decrease the effective size of the bottleneck region and therefore, affect ion diffusion. Furthermore, when an ion channel is controlled by more than one fluctuating bottleneck, diffusion can also be affected by correlations among bottlenecks [19].

Dynamic disorder is also important in the studies of glassy systems who have a broad spectrum of time scales with no clear separation between fast and slow degrees of freedom. The dynamic behavior of primary collective degrees of freedom may be coupled to other modes which follow the dynamics only on slightly shorter (or longer) time scale.

The equilibrium behavior of glassy systems is studied by the ''replica trick'' [38]. The existence of many minima of the free-energy landscape, unrelated by symmetry, gives rise in the mean-field treatment to ''replica symmetry breaking.'' This transition can be understood in terms of the extremal statistics of the Boltzmann weights of the low-lying states [38]. Their glassy dynamics are exhibited by lack of ergodicity, violation of the fluctuation-dissipation relation, and aging. The correlation and response functions depend separately on the initial and final times and not on their difference alone [39]. This transition was found for the mean first passage time of a random walk on a random Cayley tree as the temperature is lowered [40].

Ranges of applicability of these mean-field results to realistic systems are still debated and alternative approaches are needed to go beyond mean-field theory. Here, we present such an approach by studying directly the effect of the noise time scales on the dynamics of a directed random walk which models drift caused by a strong external field. In the absence of noise, the behavior is simple: the walker hops to the right to its neighboring site with a site independent rate. The distance covered varies linearly in time and the velocity is given by the intersite distance to the hopping time ratio. The dynamic disorder is modeled by coupling of the walk to a parallel channel. Despite the simplicity of this system, a very rich variety of possible behaviors is found when time scales of diffusion and fluctuation of the environment are entangled.

Random walks which serve as intuitive physical models for propagation of excitation or material transport in con-

 

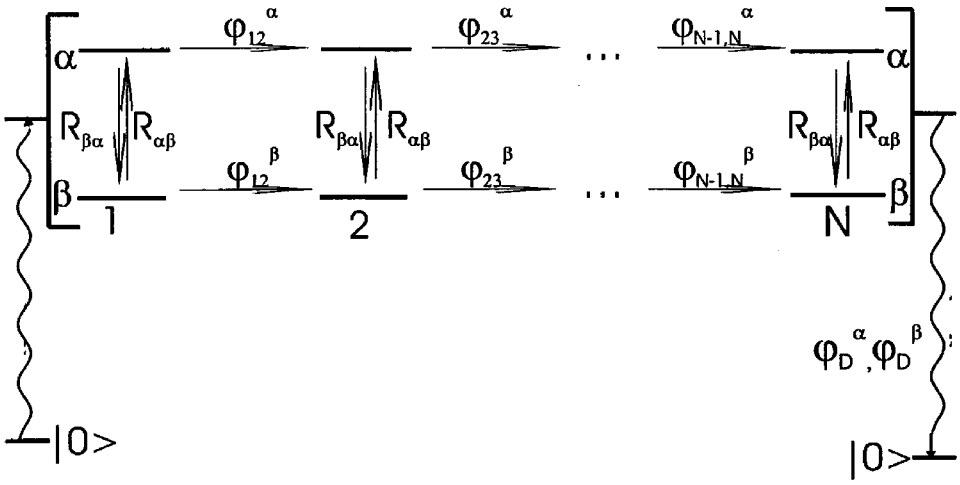


FIG. 1. Continuous time random walk among $N$ sites in the presence of dynamic disorder represented by jumps between bath states $\alpha$ and $\beta$: excitation is created in the first site, which undergoes a transition from the ground $|0\rangle$ to the excited $|1\rangle$ state, and is destroyed after it arrives to the terminal site $N$.

densed phases [5–9], may exhibit long tails in the distribution of various quantities. The directed walk considered here involves a single walker hopping to the next nearest neighbor on a line with $N$ sites and is a limiting case of the usual random walk when a jump back to the previous site can be neglected. It can be used to model excitation or material transport subject to an external potential. The probability density of making a jump is given by waiting time distributions. When these distributions are exponential, the directed walks may be described by an ordinary master equation with random transition rates. For example, the directed walls can be used to model pulling of single DNA molecules by motor proteins in bacteriophages [41].

In this paper, we model fluctuations of the environment by the bath undergoing jumps between two states, one favoring transport whereas the other acts as a trap. In many cases, environment degrees of freedom can be modeled by two relevant states [42–47]. For instance, when the diameter of a bottleneck (or dimensions of the gate of a skeleton fence) exceeds or equal to the characteristic size of diffusing entities (ions, protein, etc.), the channel (gate) is open, otherwise it is closed [48]. When the overlap of donor and acceptor wave functions is nonvanishing, the charge hops to the nearest neighbor. When this overlap is zero, charge transfer is prohibited. In this dynamic gating picture, ''the door'' stochastically fluctuates between open or closed states.

While the scaling properties of one-dimensional random walks in the presence of static disorder, i.e., the distribution of transition rates for various sites in the chain, have been extensively studied by many authors [49–51], dynamic disorder is less studied. The simple one-dimensional random walk was studied in the presence of dynamic and static disorder when fluctuations are either fast or slow than the diffusion itself [49,52]. However, modeling the intermediate regime is more difficult. We have previously analyzed the distribution of excitation arrival times for a donor-acceptor system coupled to a two-state jump bath [12]. We show that a directed random walk in an $N$-site donor-bridge-acceptor system with exponential waiting time distributions for hopping between nearest-neighboring sites acquires memory for previously visited sites in the presence of dynamic disorder.

Our model is defined in Sec. II. In Sec. III, we employ a generating Green function method to compute the distribution of probability of quenching times. In Sec. IV, we simulate the quenching time distribution and study the scaling of the mean and second moment of quenching time with $N$. The distribution of particle coordinate, its average, the distribution of second moments of coordinate, and its average are studied in Sec. V. We also compute the distribution of velocity and diffusion coefficient and their average. Our results are discussed in Sec. VI. The generating function for the recursive computation of Green functions is given in the Appendix.

## II. THE MODEL

Consider an $N$-site donor-bridge-acceptor system, where an excitation is created on the donor site (see Fig. 1), hops through bridge sites $2,\ldots,N-1$, and finally reaches the terminal site $N$ where it is quenched. The excitation transfer process is coupled to a fluctuating environment modeled by the two-state jump bath with states $\alpha$ and $\beta$ [43]. We assume a directed continuous time walk with nearest-neighbor hopping from site $i$ to $i+1$ determined by the waiting time distribution functions $\psi_i^{\alpha}(t),\psi_i^{\beta}(t)$ for the excitation jumps ($i=1,\ldots,N-1$) when the bath is in state $\mu=\alpha$ or $\beta$. Bath fluctuations are described by the rates $R_{\alpha\beta}$ and $R_{\beta\alpha}$ of $\beta\rightarrow\alpha$ and $\alpha\rightarrow\beta$ jumps, respectively, and are independent of the excitation. Finally, the quenching of excitation from states $|N\alpha\rangle$ and $|N\beta\rangle$ of the terminal site is described by the waiting time distributions $\psi_D^{\alpha}(t)$ and $\psi_D^{\beta}(t)$.

The time evolution of directed walk probabilities $P^{[i]}(t)$ of finding excitation in site $i=1,2,\ldots,N$ is described by the generalized master equations which in matrix form are given by

$$\dot{\mathbf{P}}(t;\mu)=\int_0^t d\tau\mathbf{\Phi}(\tau;\mu)\mathbf{P}(t-\tau;\mu), \tag{1}$$

where $\mu=\alpha,\beta$ and $\mathbf{P}(t;\mu)$ denotes the vector of populations of sites $i=1,2,\ldots,N$ with vector components $\mathbf{P}^{[i]}(t;\mu)$ defined by

$$\mathbf{P}^{[i]}(t;\mu)\equiv\begin{pmatrix} P_{\alpha}^{[i]}(t) \\ P_{\beta}^{[i]}(t) \end{pmatrix} \tag{2}$$

$\mathbf{\Phi}(t;\mu)$ is a $N\times N$ two-block-diagonal matrix of $2\times 2$ matrix $\mathbf{\Phi}^{(i)}(t;\mu)$ of generalized rates of excitation transfer and bath jump rate matrix $\mathbf{R}$,

$$\mathbf{\Phi}(t,\mu)=\begin{pmatrix} -\mathbf{\Phi}^{(1)}(t;\mu)-\mathbf{R} & 0 & \cdots & 0 \\ \mathbf{\Phi}^{(1)}(t;\mu) & -\mathbf{\Phi}^{(2)}(t;\mu)-\mathbf{R} & \cdots & 0 \\ 0 & \cdots & \mathbf{\Phi}^{(N-1)}(t;\mu) & -\mathbf{\Phi}^{(D)}(t;\mu)-\mathbf{R} \end{pmatrix}, \tag{3}$$

where

$$\mathbf{\Phi}^{(i)}(t;\mu)=\begin{pmatrix} \phi_i^{\alpha}(t) & 0 \\ 0 & \phi_i^{\beta}(t) \end{pmatrix}, \tag{4}$$

$$\mathbf{\Phi}^{(D)}(t;\mu)=\begin{pmatrix} \phi_D^{\alpha}(t) & 0 \\ 0 & \phi_D^{\beta}(t) \end{pmatrix}, \tag{5}$$

and

$$\mathbf{R}=\begin{pmatrix} R_{\alpha\beta} & -R_{\beta\alpha} \\ -R_{\alpha\beta} & R_{\beta\alpha} \end{pmatrix}. \tag{6}$$

Using the Laplace transformation

$$\tilde{f}(z)\equiv\int_0^{\infty} dt e^{-zt} f(t), \tag{7}$$

the matrix elements of Eqs. (4) and (5) may be computed in terms of the waiting time distributions

$$\tilde{\phi}_i^{\alpha,\beta}(z)=z\tilde{\psi}_i^{\alpha,\beta}(z)[1-\tilde{\psi}_i^{\alpha,\beta}(z)]^{-1}, \tag{8}$$

$$\tilde{\phi}_D^{\alpha,\beta}(z)=z\tilde{\psi}_D^{\alpha,\beta}(z)[1-\tilde{\psi}_D^{\alpha,\beta}(z)]^{-1}. \tag{9}$$

With the choice $\psi_i(t,\mu)=k_i^{\mu}\exp\{-k_i^{\mu}t\}$ for $i=1,2,\ldots,N$ and $\psi_Q(\tau;\mu)=k_D^{\mu}\exp\{-k_D^{\mu}t\}$, $\mathbf{\Phi}(t)$ reduces to the ordinary kinetic rate matrix with $\phi_i(\mu)=k_i^{\mu}$ and $\phi_Q(\mu)=k_D^{\mu}$, and Eqs. (16) become ordinary master equations, i.e., $\dot{\mathbf{P}}(t,\mu)=\mathbf{\Phi}(\mu)\mathbf{P}(t,\mu)$.

The generalized master equations (1) may be solved by defining the conditional probability matrix $\mathbf{G}$ for the excitation to reside in state $|j\mu\rangle$ at time $t'$ given that excitation was in state $|i\nu\rangle$ at earlier time $t$ ($i,j$ and $\mu,\nu$ denote sites $1,2,\ldots,N$ and bath states $\alpha,\beta$, respectively), i.e.,

$$\mathbf{G}(t,i\nu;t',j\mu)\equiv[G(t-t';0)]_{\{i\nu\},\{j\mu\}}, \tag{10}$$

where $i\mu=i\alpha,i\beta$ is the site and bath state dependent index. $\mathbf{P}^{[i]}(t;\mu)$ can then be expressed as

$$\mathbf{P}^{[i]}(t;\mu)=\mathbf{P}(t;i\mu)=\sum_{j\mu}\mathbf{G}(t,i\nu;0,j\mu)\mathbf{P}(0;j\mu), \tag{11}$$

where $\mathbf{P}(0;j\mu)$ is the probability to find excitation in state $|j\mu\rangle$ at time $t=0$. $\mathbf{G}$ is given in Laplace domain by

$$\tilde{\mathbf{G}}(z;\mu)=[z\mathbf{I}-\tilde{\mathbf{\Phi}}(z;\mu)]^{-1}, \tag{12}$$

and $\mathbf{P}(t;\mu)$ is obtained by inverse Laplace ($L^{-1}:z\rightarrow t$) transform and substituting $\mathbf{G}(t;\mu)$ back into Eq. (12).

To study the scaling of quenching times with $N$, we need to compute the Green functions, Eq. (12). Because excitation is created in site 1, a $2\times 2$ matrix of Green functions $G_{\mu\nu}^{[N]}(t)$ is formed by elements of the $2N\times 2N$ matrix $L^{-1}\{[z\mathbf{I}-\tilde{\mathbf{\Phi}}(z;\mu)]^{-1}\}$ of propagators of excitation from state $|1\mu\rangle$ to state $|N\nu\rangle$ ($\mu\nu=\alpha,\beta$). There are in total $2^{N-1}$ bath state dependent pathways for propagation of excitation represented by $2^{N-1}$ diagrams for each of the propagators $\tilde{G}_{\mu\nu}^{[N]}(z)$ ($\mu\nu=\alpha,\beta$) resulting in total of $2^N$ possible diagrams representing propagators $z+\tilde{\phi}^{\beta}{}_i(z)+R_{\beta\alpha}$ and $z+\tilde{\phi}^{\alpha}{}_i(z)+R_{\alpha\beta}$ of excitation in states $|i\alpha\rangle$ and $|j\beta\rangle$, excitation hops from site $i$ to site $i+1$ while being in state $\alpha$ or $\beta$ described by the generalized rates $\tilde{\phi}^{\alpha}{}_i(z)$ or $\tilde{\phi}^{\beta}{}_i(z)$, and bath jumps rates. These fragments are presented in Fig. 2 (panel *A*). In each diagram, the number of propagators $p$ plus the number of bath jumps $N-p$ is equal to the total number of sites $N$. The number of diagrams with $p$ propagators and $N-p$ bath jumps is given by the binomial distribution $C_N^p=N!/[p!(N-p)!]$. Diagonal elements of the Green function matrix, $\tilde{G}_{\alpha\alpha}^{[N]}(z)$ and $\tilde{G}_{\beta\beta}^{[N]}(z)$, have either even number of bath jumps or zero. Off-diagonal elements, $\tilde{G}_{\alpha\beta}^{[N]}(z)$ and $\tilde{G}_{\beta\alpha}^{[N]}(z)$, have either odd number of jumps or zero. Some of the diagrams for computation of Green functions $\tilde{G}_{\alpha\alpha}^{[N]}(z)$ and $\tilde{G}_{\alpha\beta}^{[N]}(z)$ for $N=2$ and 3 are given in Fig. 2 (panel *B*).

The entire distribution of quenching probabilities for arbitrary $N$ is obtained by summing over all $2^{N-1}$ diagrams for each of the four elements of Green function matrix. This matrix can be obtained numerically by diagonalizing the matrix $\mathbf{\Phi}(t)$ itself when the waiting time distributions $\psi$'s are exponential or finding the inverse of matrix $[z\mathbf{I}-\tilde{\mathbf{\Phi}}(z)]$ for general $\psi$'s followed by inverse Laplace transformation to the time domain. It becomes a formidable task for large $N$.

We have computed the Green functions for the $N$-site problem recursively starting from Green functions for a single site using a generating function approach outlined in the Appendix. The Green functions for the $N$-site problem are given by

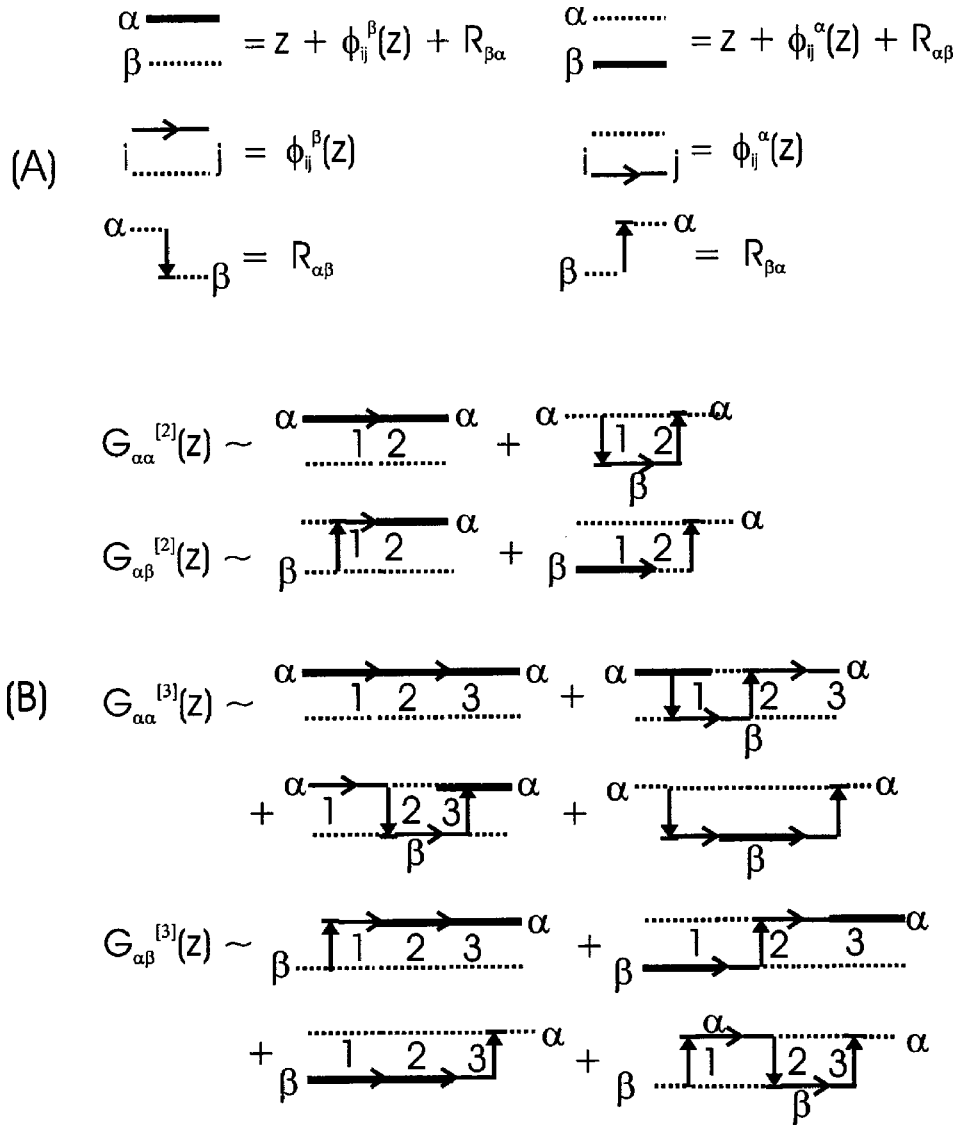


FIG. 2. Panel *A*: propagators, waiting time distributions for excitation jumps $i\alpha \to j\alpha$ and $i\beta \to j\beta$ and bath jumps $i\alpha \to i\beta$ and $i\beta \to i\alpha$. Panel *B*: Green functions $\tilde{G}_{\alpha\alpha}^{[N]}(z)$ and $\tilde{G}_{\alpha\beta}^{[N]}(z)$ for calculation of the excitation population the last site for $N=2$ and $N=3$.

$$\begin{pmatrix} \tilde{G}_{\alpha\alpha}^{[N]}(z) \\ \tilde{G}_{\alpha\beta}^{[N]}(z) \end{pmatrix} = \begin{pmatrix} \tilde{\lambda}_1^{N-1}(z) & 0 \\ 0 & \tilde{\lambda}_2^{N-1}(z) \end{pmatrix} \begin{pmatrix} \tilde{G}_{\alpha\alpha}^{[1]}(z) \\ \tilde{G}_{\alpha\beta}^{[1]}(z) \end{pmatrix}, \quad (13)$$

where $\tilde{G}_{\alpha\alpha}^{[1]}(z)$ and $\tilde{G}_{\alpha\beta}^{[1]}(z)$ are single site Green functions and $\tilde{\lambda}_1(z)$, $\tilde{\lambda}_2(z)$ are the eigenvalues of the generating matrix $\tilde{\mathbf{A}}_n(z)$ given by Eq. (A2).

All our calculations were carried out using Eq. (13). It shows that the Green functions for the excitation transfer process can be computed from the Green functions for the two-eigenchannel problem in which this excitation is created and destroyed on a single site.

### III. QUENCHING PROBABILITY DISTRIBUTIONS

We now study a directed walk with no disorder so that $\psi_i^{\alpha,\beta} = \psi^{\alpha,\beta}$ for $i=1,2,\ldots,N-1$. Assuming exponential waiting time distribution

$$\psi^{\alpha,\beta}(t) = k^{\alpha,\beta} e^{-k^{\alpha,\beta}t}, \quad (14)$$

$$\psi_D^{\alpha,\beta}(t) = k_D^{\alpha,\beta} e^{-k_D^{\alpha,\beta}t}, \quad (15)$$

and using Eqs. (13), we have computed probabilities $Q_\alpha^{[N]}(t)$ and $Q_\alpha^{[N]}(t)$ of excitation quenching from terminal states $|N\alpha\rangle$ and $|N\beta\rangle$ after it has been created in site 1 at time $t=0$ defined by

$$\begin{pmatrix} Q_\alpha^{[N]}(t) \\ Q_\beta^{[N]}(t) \end{pmatrix} \equiv \begin{pmatrix} k_D^\alpha & 0 \\ 0 & k_D^\beta \end{pmatrix} \begin{pmatrix} G_{\alpha\alpha}^{[N]}(t) & G_{\alpha\beta}^{[N]}(t) \\ G_{\beta\alpha}^{[N]}(t) & G_{\beta\beta}^{[N]}(t) \end{pmatrix} \begin{pmatrix} w_{eq}^\alpha \\ w_{eq}^\beta \end{pmatrix}, \quad (16)$$

where $w_{eq}^\alpha = R_{\alpha\beta}/(R_{\alpha\beta}+R_{\beta\alpha})$, $w_{eq}^\beta = R_{\beta\alpha}/(R_{\alpha\beta}+R_{\beta\alpha})$ are equilibrium populations of states $|1\alpha\rangle$ and $|1\beta\rangle$ of the first site, respectively, and the average quenching probability $\langle Q^{[N]}(t)\rangle$ given by

$$\langle Q^{[N]}(t)\rangle = Q_\alpha^{[N]} + Q_\beta^{[N]}. \quad (17)$$

We computed $Q_\alpha^{[N]}(t)$, $Q_\beta^{[N]}(t)$, and $\langle Q^{[N]}(t)\rangle$ for the models $M1-M9$ of fast and slow channels, i.e., $k^\alpha \ll k^\beta$. Models $M1-M9$ are summarized in Table I. We set $k_D^\alpha$

TABLE I. Parameters of models $M1-M12$ used in Figs. 3–12.

| Model | $k^{\alpha}$ | $k^{\beta}$ | $R_{\alpha\beta}$ | $R_{\beta\alpha}$ | $k_{\mathrm{D}}^{\alpha}$ | $k_{\mathrm{D}}^{\beta}$ |
|---|---|---|---|---|---|---|
| $M1$ | 1.0 | 7.0 | 0.1 | 0.1 | $1.0\times10^{2}$ | $1.0\times10^{2}$ |
| $M2$ | 1.0 | 7.0 | 1.0 | 1.0 | $1.0\times10^{2}$ | $1.0\times10^{2}$ |
| $M3$ | 1.0 | 7.0 | 25.0 | 25.0 | $1.0\times10^{2}$ | $1.0\times10^{2}$ |
| $M4$ | 1.0 | 7.0 | 0.1 | 0.4 | $1.0\times10^{2}$ | $1.0\times10^{2}$ |
| $M5$ | 1.0 | 7.0 | 1.0 | 4.0 | $1.0\times10^{2}$ | $1.0\times10^{2}$ |
| $M6$ | 1.0 | 7.0 | 20.0 | 80.0 | $1.0\times10^{2}$ | $1.0\times10^{2}$ |
| $M7$ | 1.0 | 7.0 | 0.4 | 0.4 | $1.0\times10^{2}$ | $1.0\times10^{2}$ |
| $M8$ | 1.0 | 7.0 | 4.0 | 1.0 | $1.0\times10^{2}$ | $1.0\times10^{2}$ |
| $M9$ | 1.0 | 7.0 | 80.0 | 20.0 | $1.0\times10^{2}$ | $1.0\times10^{2}$ |
| $M10$ | 1.0 | 10.0 | 0.05 | 0.05 | | |
| $M11$ | 1.0 | 10.0 | 0.5 | 0.5 | | |
| $M12$ | 1.0 | 10.0 | 50.0 | 50.0 | | |

$=k_D^{\beta}=k_D$ and assumed that quenching is fast compared with excitation transfer and bath jumps, i.e., $k_D \gg k,R$ and when bath jumps are slow $\kappa \gg 1$ ($M1$, $M4$, and $M7$), intermediate $\kappa \sim 1$ ($M2$, $M5$, and $M8$), and fast $\kappa \ll 1$ ($M3$, $M6$, and $M9$) compared with excitation hopping rate $K^{\alpha,\beta}$ which in the case of exponential waiting time distributions of Eq. (14) is given by

$$K^{\alpha,\beta}=\frac{\int_0^{\infty} dt\,\psi^{\alpha,\beta}(t)}{\int_0^{\infty} dt\,\psi^{\alpha,\beta}(t)t}=k^{\alpha,\beta}. \tag{18}$$

In models $M1-M3$, $R_{\alpha\beta}=R_{\beta\alpha}$. In models $M4-M6$, $R_{\beta\alpha}<R_{\alpha\beta}$, where bath state $\beta$ facilitating faster transfer, and in models $M7-M9$, $R_{\beta\alpha}>R_{\alpha\beta}$.

In Fig. 3, we display $Q_{\alpha}^{[N]}(t)$, $Q_{\alpha}^{[N]}(t)$, and $\langle Q^{[N]}(t)\rangle$ for models $M1-M3$ and $N=4$, 10, and 20. For larger $N$, peaks of probabilities shift toward longer times. Plots of $Q_{\alpha}^{[N]}(t)$, $Q_{\alpha}^{[N]}(t)$, and $\langle Q^{[N]}(t)\rangle$ for models $M1$ and $M2$ exhibit long tails which gradually disappear as jump rates increase as we move from $M1$ to $M2$ and to $M3$. Note the remarkable difference in the time profile of $Q_{\alpha}^{[N]}(t)$ and $Q_{\beta}^{[N]}(t)$ for models $M1$ and $M2$. This is not the case for $M3$ as $Q_{\alpha}^{[N]}(t)$ differs from $Q_{\beta}^{[N]}(t)$ only in the amplitude. Because "fast channel" primarily contributes to excitation quenching, $\langle Q^{[N]}(t)\rangle$ resembles $Q_{\alpha}^{[N]}(t)$.

Models $M4-M6$ are depicted in Fig. 4. Here, fast channel is less populated as excitation transfers to the terminal site $N=4$, 10, and 20 and the weights of $Q_{\alpha}$ and $Q_{\beta}$ in $\langle Q\rangle$ are roughly equal. After creation of excitation in site 1 at $t=0$, the fast channel probability quickly passes the probability in slow channel. Coupling between these channels makes faster (slower) part to decay from the terminal site at shorter

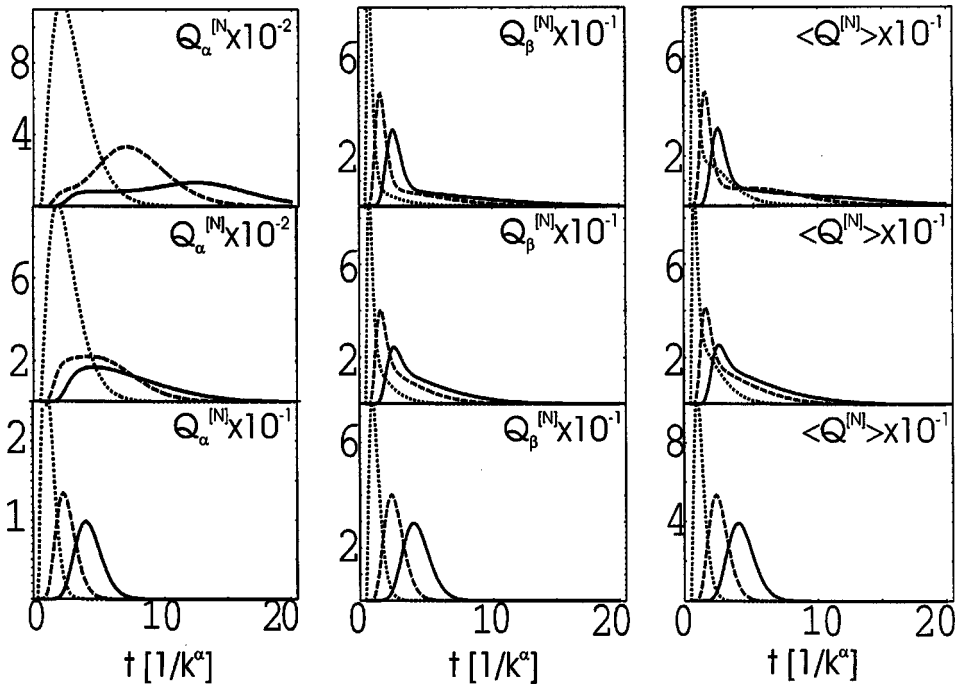


FIG. 3. Distribution of excitation quenching probabilities $Q_{\alpha}^{[N]}(t)$ (left panels) and $Q_{\beta}^{[N]}(t)$ (middle panels) of the terminal site states $|N\alpha\rangle$ and $|N\beta\rangle$ and the average quenching probability $Q^{[N]}(t)$ (right panels) for $N=4$ (dashed lines), 10 (dotted lines), and 20 (solid lines) for models $M1$ (top), $M2$ (middle), and $M3$ (bottom).

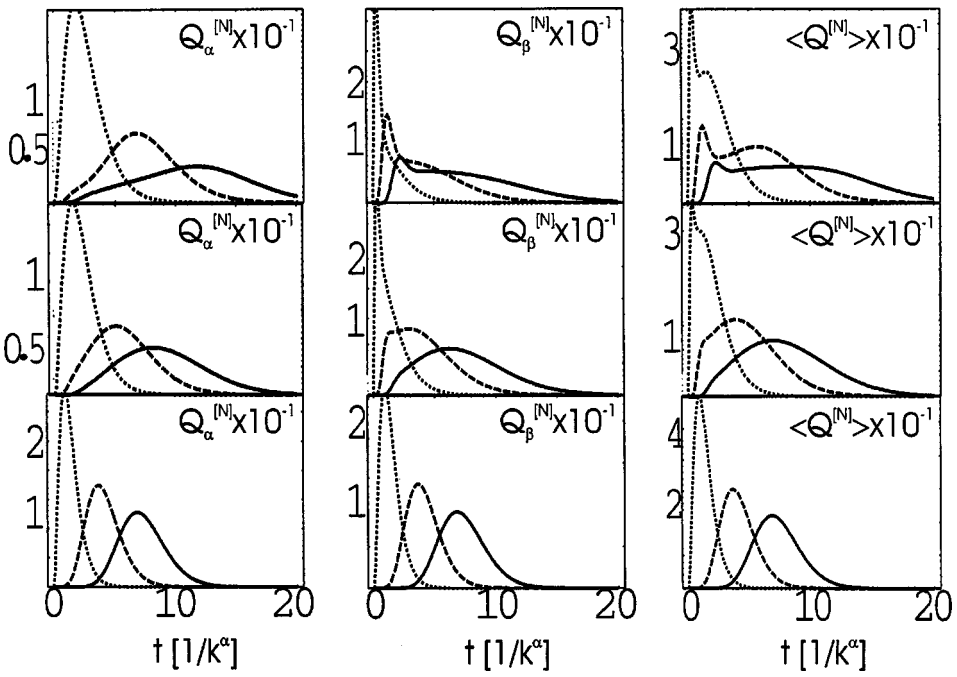


FIG. 4. Distribution of excitation quenching probabilities $Q_\alpha^{[N]}(t)$ (left panels) and $Q_\beta^{[N]}(t)$ (middle panels) of the terminal site states $|N\alpha\rangle$ and $|N\alpha\rangle$ and the average quenching probability $Q^{[N]}(t)$ (right panels) for $N=4$ (dashed lines), 10 (dotted lines), and 20 (solid lines) for models $M4$ (top), $M5$ (middle), and $M6$ (bottom).

(longer) times which shows up in the double-peaked feature of $\langle Q^{[N]}(t)\rangle$ for model $M4$. The shorter time peak becomes more of a cusp for model $M5$ and disappears altogether for model $M6$.

Comparing Figs. 3 and 4, we see that $Q_\alpha$, $Q_\beta$, and $\langle Q\rangle$ for slow and intermediate bath exhibit power-law tails. This implies that excitation transfer retains memory to its initial state. In fact, using the eigenchannel picture of the Appendix, $\tilde{Q}_\alpha^{[N]}(z)$ and $\tilde{Q}_\alpha^{[N]}(z)$ can be recast as

$$\begin{pmatrix} \tilde{Q}_\alpha^{[N]}(z) \\ \tilde{Q}_\beta^{[N]}(z) \end{pmatrix} = k_D \begin{pmatrix} \tilde{\lambda}_1^{N-1}(z) & 0 \\ 0 & \tilde{\lambda}_2^{N-1}(z) \end{pmatrix} \begin{pmatrix} \tilde{G}_{\alpha\alpha}^{[1]}(z) & \tilde{G}_{\alpha\beta}^{[1]}(z) \\ \tilde{G}_{\beta\alpha}^{[1]}(z) & \tilde{G}_{\beta\beta}^{[1]}(z) \end{pmatrix} \times \begin{pmatrix} w_{eq}^\alpha \\ w_{eq}^\beta \end{pmatrix}, \tag{19}$$

with the eigenvalues $\tilde{\lambda}_1(z)$ and $\tilde{\lambda}_2(z)$ given by

$$\tilde{\lambda}_{1,2}(z) = \frac{1}{2\det[\tilde{\mathbf{M}}(z)]}\{2k^\alpha k^\beta + R\langle k\rangle + zK \pm \sqrt{(2k^\alpha k^\beta + R\langle k\rangle + zK)^2 - 4k^\alpha k^\beta[z^2 + z(R+K) + k^\alpha k^\beta + R\langle k\rangle]}\}, \tag{20}$$

where the average rate $\langle k\rangle$ is defined by $\langle k\rangle = w_{eq}^\alpha k^\alpha + w_{eq}^\beta k^\beta$, $R = R_{\alpha\beta} + R_{\beta\alpha}$, $K = k^\alpha + k^\beta$, and

$$\tilde{\mathbf{M}}(z) = \begin{pmatrix} z + k^\alpha + R_{\beta\alpha} & R_{\beta\alpha} \\ R_{\alpha\beta} & z + k^\beta + R_{\alpha\beta} \end{pmatrix}. \tag{21}$$

Taking inverse Laplace transform of Eq. (19), we obtain

$$Q_\alpha^{[N]}(t) = w_{eq}^\alpha \int_0^t d\tau\, \lambda_1^{N-1}(\tau) Q_{\alpha\alpha}^{[1]}(t-\tau) + w_{eq}^\beta \int_0^t d\tau\, \lambda_2^{N-1}(\tau) Q_{\alpha\beta}^{[1]}(t-\tau), \tag{22}$$

$$Q_\beta^{[N]}(t) = w_{eq}^\alpha \int_0^t d\tau\, \lambda_1^{N-1}(\tau) Q_{\beta\alpha}^{[1]}(t-\tau) + w_{eq}^\beta \int_0^t d\tau\, \lambda_2^{N-1}(\tau) Q_{\beta\beta}^{[1]}(t-\tau).$$

$Q_{\mu\nu}^{[1]}(t)$ $(\mu\nu = \alpha,\beta)$ in Eq. (22) represent memoryless propagation of excitation on a single site. Memory effects enter the dynamics through the eigenvalues $\tilde{\lambda}_1(z)$ and $\tilde{\lambda}_2(z)$ taken to power $N-1$ which in the time domain become integral memory kernels $\lambda_1^{N-1}(t)$ and $\lambda_2^{N-1}(t)$.

Note that when $R_{\alpha\beta} = R_{\beta\alpha} = 0$, $\tilde{G}_{\alpha\beta}^{[1]}(z)$ and $\tilde{G}_{\beta\alpha}^{[1]}(z)$ vanish and eigenvalues (20) of transformation (A2) are given by $\tilde{\lambda}_1^0(z) = k^\alpha/(z+k^\alpha)$ and $\tilde{\lambda}_2^0(z) = k^\beta/(z+k^\beta)$, where superscript "0" denotes no disorder. The distribution of quenching probability becomes

$$[Q_\mu^{[N]}]^0(t)=P_\mu(0)\frac{\Gamma(N-1)-\Gamma(N-1,(k^\mu-k_D)t)}{\Gamma(N-1)(k^\mu-k_D)^{N-1}}e^{-k_Dt},$$

$$\mu=\alpha,\beta, \tag{23}$$

where $P_\mu(0)$ is a populations of state $|1\mu\rangle$ at time $t=0$, $\Gamma(N)=(N-1)!$, and $\Gamma(N,y)$ is defined by

$$\Gamma(N,y)\equiv\int_y^\infty dte^{-t}t^{N-1}, \tag{24}$$

In particular, when $k^\mu=k_D$, Eq. (23) gives $[Q_\mu^{[N]}]^0(t)=P_\mu(0)\Gamma^{-1}(N)\ [k^\mu]^Nt^{N-1}\exp\{-k^\mu t\}$. It follows from Eq. (23) that in the absence of dynamic disorder excitation quenching probability is exponentially distributed.

From Figs. 3 and 4, we see that the dynamic disorder self-averages for fast bath jump models $M3$ and $M6$. As a result, aside from the overall amplitude $Q_\alpha^{[N]}(t)$, $Q_\alpha^{[N]}(t)$, and $\langle Q^{[N]}(t)\rangle$ are identical. Invoking eigenchannel representation, the eigenvalues (20) of transformation (A2) in the limit of fast bath jumps become $\tilde\lambda_1^{fb}(z)=0$ and $\tilde\lambda_2^{fb}(z)=\langle k\rangle/(z+\langle k\rangle)$, where $R\equiv R_{\alpha\beta}+R_{\beta\alpha}$ and the superscript "$fb$" denotes fast bath. Vanishing $\tilde\lambda_1^{fb}$ implies that we no longer have two interacting eigenchannels $\alpha$ and $\beta$ but rather, the dynamics of quenching probability is now averaged. As a result, excitation hops in the "averaged channel" with the average rate $\langle k\rangle$ and the average quenching probability

$$\langle Q^{[N]}(t)\rangle^{fb}=\frac{\Gamma(N-1)-\Gamma(N-1,(\langle k\rangle-k_D)t)}{\Gamma(N-1)(\langle k\rangle-k_D)^{N-1}}e^{-k_Dt}. \tag{25}$$

The distribution of quenching probability can be computed as $[Q_\mu^{[N]}]^{fb}(t)=w_{eq}^\mu\langle Q^{[N]}(t)\rangle^{fb}$. In particular, when $\langle k\rangle=k_D$, we obtain $\langle Q^{[N]}(t)\rangle^{fb}=\Gamma^{-1}(N)\ \langle k\rangle^Nt^{N-1}\exp\{-\langle k\rangle t\}$. In the limit of large $N$, $\langle Q^{[N]}(t)\rangle^{fb}$ becomes a Gaussian distribution,

$$\langle Q^{[N]}(t)\rangle^{fb}\approx\frac{\langle k\rangle}{\sqrt{2\pi N}}\exp\left[-\frac{[t-N/\langle k\rangle]^2}{2N/\langle k\rangle^2}\right]\quad\text{for large } N, \tag{26}$$

which is a consequence of the central limit theorem. When $N\to\infty$, the relative width of $\langle Q^{[N]}(t)\rangle^{fb}$, $(\sqrt{N}/\langle k\rangle)/(N/\langle k\rangle)$ approaches zero and excitation transport becomes a self-averaging deterministic process.

Therefore, both in the fast bath jump limit when the dynamic disorder self-averages and in the absence of dynamic disorder, the distribution of quenching probability, given by Eqs. (23) and (25) respectively, is exponential and the $N$-site walk can be described as a Markovian process without including explicitely the bath variable. However, when $\kappa N\sim1$ (dynamic disorder), the distribution of quenching probability is governed by Eqs. (22) with nontrivial memory kernels $\lambda_1^{N-1}(t)$ and $\lambda_2^{N-1}(t)$, and excitation transfer becomes a non-Markovian walk with memory. For models $M7-M9$ (not shown), we found that the time profile of $\langle Q^{[N]}(t)\rangle$ is dominated by a contribution from a fast channel.

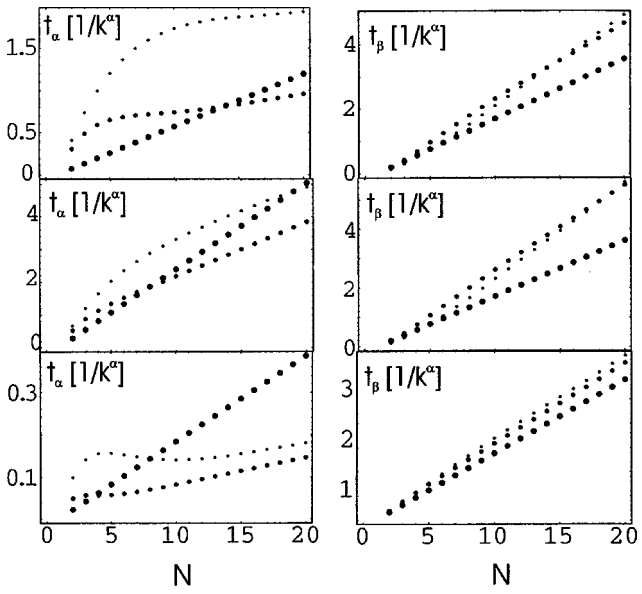


FIG. 5. Partial first moments $t_\alpha$ (left panels) and $t_\beta$ (right panels) of quenching time vs $N$ for models $M1-M3$ (top), $M4-M6$ (middle), and $M7-M9$ (bottom). Size of circles increases with bath jump rates: small, intermediate, and large circles represent $\kappa\gg1$, $\kappa\sim1$, and $\kappa\ll1$, respectively.

## IV. DISTRIBUTION OF QUENCHING TIMES

Using Eqs. (16) for the probability distribution of quenching times, we now compute its partial moments ($p=1,2,\ldots$),

$$t_\nu^{(p)}(N)\equiv\int_0^\infty dtQ_\nu^{[N]}(t)t^p,\quad\nu=\alpha,\beta, \tag{27}$$

$t_\nu^{(p)}$ is the $p$th moment corresponding to quenching from state $|N\nu\rangle$. The total moment of quenching time distribution is given by

$$\langle t^{(p)}(N)\rangle=t_\alpha^{(p)}(N)+t_\beta^{(p)}(N). \tag{28}$$

In Fig. 5, we display partial first moments $t_\alpha(N)$, $t_\beta(N)$ of the quenching time vs $N$ for models $M1-M9$. Because in these models $k_D\gg k,R$, $t_\alpha(N)$, and $t_\beta(N)$ and the mean quenching time (MQT) $\langle t(N)\rangle$ studied below are equivalent to partial first moments of passage time and the mean-first passage time, respectively. $t_\alpha(N)$ and $t_\beta(N)$ for models $M1$, $M4$, $M7$ ($\kappa\gg1$) and $M2$, $M5$, $M8$ ($\kappa\sim1$) exhibit nonlinear scaling with $N$. Only when the dynamic disorder averages out, do $t_\alpha(N)$ and $t_\beta(N)$ scale linearly with $N$ for models $M3$, $M6$, and $M9$ ($\kappa\ll1$). Note that $t_\beta(N)$ (fast channel) approaches linear scaling faster than $t_\alpha(N)$.

Before analyzing the MQT for models $M1-M9$, let us examine the limiting cases of no dynamic disorder ($\kappa\to\infty$) or fast bath jumps ($\kappa\to0$) considered in the preceding sec-

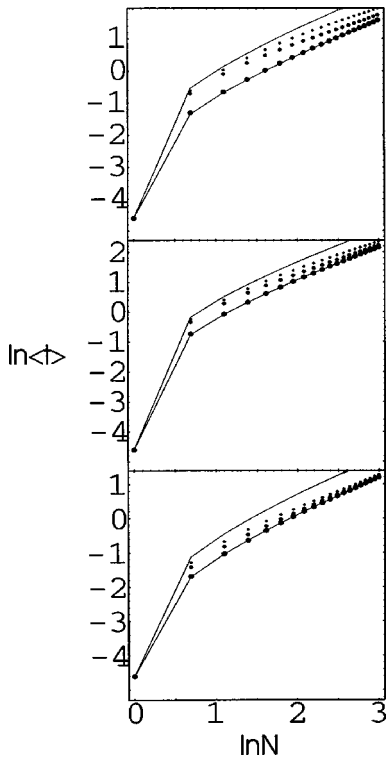


FIG. 6. Log-log plots of the mean quenching time vs $N$ for models $M1-M3$ (top panel), $M4-M6$ (middle panel), and $M7-M9$ (bottom panel). Size of circles increases with bath jump rates (see Fig. 5). Upper curves reflect scaling with no disorder $\langle t\rangle_0$. Lower curves are obtained for fast bath jumps $\langle t\rangle_{fb}$.

tion. Using the distribution of quenching probability given by Eqs. (23) and (25) in Eqs. (27) and (28) and setting $p=1$, we obtain

$$\langle t(N)\rangle_0 = A_0 N + B_0, \tag{29}$$

$$\langle t(N)\rangle_{fb} = A_{fb} N + B_{fb},$$

where the coefficients $A_0$, $B_0$, $A_{fb}$, and $B_{fb}$ are given by

$$A_0 = \frac{1}{k^\alpha} P_\alpha(0) + \frac{1}{k^\beta} P_\beta(0), \tag{30}$$

$$B_0 = \left(\frac{1}{k_D^\alpha} - \frac{1}{k^\alpha}\right) P_\alpha(0) + \left(\frac{1}{k_D^\beta} - \frac{1}{k^\beta}\right) P_\beta(0),$$

$$A_{fb} = \langle k\rangle^{-1},$$

$$B_{fb} = \frac{1}{\langle k_D\rangle} - \frac{1}{\langle k\rangle},$$

and the average excitation quenching rate $\langle k_D\rangle$ is given by $\langle k_D\rangle = w_{eq}^\alpha k_D^\alpha + w_{eq}^\beta k_D^\beta$. Therefore, for a Markovian random walk in the limit $\kappa\to\infty$ or $\kappa\to 0$, the MQT $\langle t(N)\rangle_0$ and $\langle t(N)\rangle_{fb}$ scale linearly with $N$. When $k_D^{\alpha,\beta} = k^{\alpha,\beta}$ and $\langle k_D\rangle = \langle k\rangle$, we obtain $\langle t(N)\rangle_0 = A_0 N$ and $\langle t(N)\rangle_{fb} = A_{fb} N$.

In Fig. 6, we present log-log plots of $\langle t(N)\rangle$ vs $N$ for models $M1-M9$. $\langle t(N)\rangle$ lie between the upper bound given by $\langle t(N)\rangle_0$ and the lower bound $\langle t(N)\rangle_{fb}$. When the time it takes for excitation to reach the site $N$ is short compared with $1/R$, i.e., when $N\kappa \gg 1$, the MQT can be reasonably approximated by $\langle t\rangle_0$. For our model parameters, $N\sim 1$ (note that both curves $\langle t\rangle_0$ and $\langle t\rangle_{fb}$ coincide with data points for models $M1-M9$ for $N=1$). In the opposite limit, $\langle t\rangle \approx \langle t\rangle_{fb}$. Therefore, models $M1-M9$ tend asymptotically to $\langle t\rangle_{fb}$ for large $N$ (in our calculation $N\sim 20$).

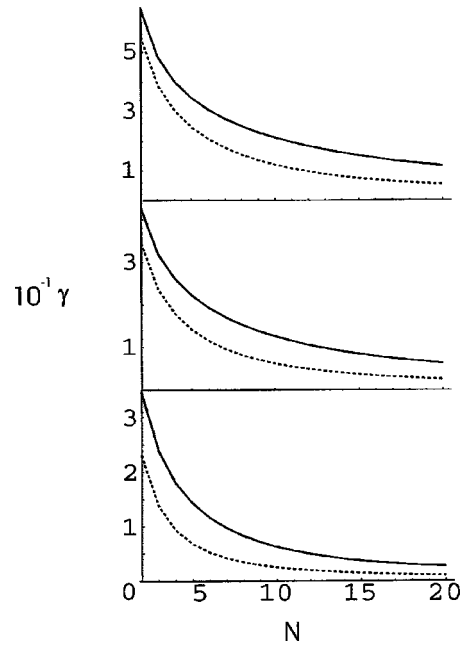


FIG. 7. Plots of the fractional exponent $\gamma$ vs $N$ for models $M1$, $M2$ (top), $M4$, $M5$ (middle), and $M7$, $M8$ (bottom). Solid (dashed) curves denote $\kappa \gg 1$ ($\kappa\sim 1$) models $M1$, $M4$, and $M7$ ($M2$, $M5$, and $M8$).

The crossover between the two asymptotic regimes is clearly observed when $N\kappa\sim 1$. Indeed, the log-log plot for this case indicates that the apparent exponent is somewhat larger than one for intermediate $N$, and only gradually approaches the scaling form $\langle t\rangle \sim N$. We have found that in this parameter regime, the MQT is described by the nonlinear scaling law

$$\langle t(N)\rangle = A_{fb} N^{1+\gamma(N)} + B_{fb}, \tag{31}$$

where $\gamma$ is the $N$-dependent fractional exponent. Therefore, in a context of the MQT the non-Markovian memory effects (e.g., long tails of the distributions of quenching probability depicted in Figs. 3 and 4) are reflected in the deviation of apparent exponent from the unity in the log-log plot of $\langle t(N)\rangle$ vs $N$.

In Fig. 7, we display the fractional exponent $\gamma$ as a function of $N$ for models $M1$, $M2$, $M4$, $M5$, $M7$, and $M8$. $\gamma$ asymptotically tends to zero for large $N$. Faster bath jumps result in smaller initial amplitude and faster decay of $\gamma$. When $N\kappa \gg 1$, the dynamic disorder self-averages and $\langle t(N)\rangle$ again approaches linear scaling. In this limit, $A_{fb}$ and $B_{fb}$ are given by the average transfer and quenching rates $\langle k\rangle$ and $\langle k_D\rangle$ [see the last two Eqs. (30)].

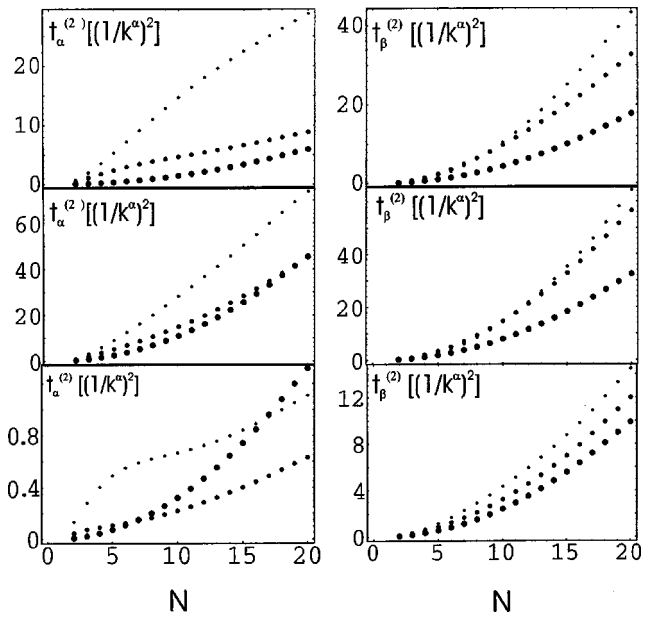


FIG. 8. Partial second moments $t_\alpha^{(2)}$ (left panels) and $t_\beta^{(2)}$ (right panels) of quenching time vs $N$ for models $M1-M3$ (top), $M4-M6$ (middle), and $M7-M9$ (bottom). Size of circles increases with bath jump rates as in Fig. 5.

Using the generating Green function technique of the previous sections and Eq. (22), we now Taylor expand Eq. (28) (with $p=1$) around $\langle t(N)\rangle_{fb}$, i.e.,

$$\langle t(N)\rangle = \langle t(N)\rangle_{fb} + \gamma\left[\frac{\partial}{\partial\gamma}\langle t(N)\rangle\right]_{\gamma=0} + 0(\gamma^2), \quad (32)$$

and to the first order in $\gamma$, we obtain

$$\gamma(N) = \kappa\frac{N-1}{N\ln N}, \quad (33)$$

Eq. (33) implies that the amplitude of $\gamma(N)$ is proportional to $\kappa$ and that $\gamma$ scales as $\gamma\sim 1/\ln N$ for large $N$. When $\kappa\to 0$, $\gamma(N)\to 0$.

We have also analyzed partial second moments of quenching time $t_\alpha^{(2)}(N)$ and $t_\beta^{(2)}(N)$ and the average second moment $\langle t^{(2)}(N)\rangle$. $t_\alpha^{(2)}$ and $t_\beta^{(2)}$ vs $N$ shown in Fig. 8 for models $M1-M9$ are similar to the distribution of first moments $t_\alpha$ and $t_\beta$ (Fig. 5). In Fig. 9, we present the log-log plots of $\langle t^{(2)}\rangle$ vs $N$ for models $M1-M9$. Again, we observe similarity in the $N$ profile between $\langle t^{(2)}\rangle$ and $\langle t\rangle$ (Fig. 5). The log-log plots also indicate that the apparent exponent is larger than two for small $N$, but asymptotically approaches the scaling form $\langle t^2\rangle\sim N^2$ for large $N$ or fast bath jumps.

In Fig. 10, we show the ratio of second moment of the MQT to the square of the MQT,

$$r(N) = \frac{\langle t^{(2)}(N)\rangle}{\langle t(N)\rangle^2}, \quad (34)$$

as a function of $N$ for models $M1-M9$. This quantity probes a contribution to quenching times from rare events. $r(N)$ starts off from a finite value (not equal to 1) and decays with $N$, approaching asymptotic value $r(N)=1$ for large $N$. Varia-

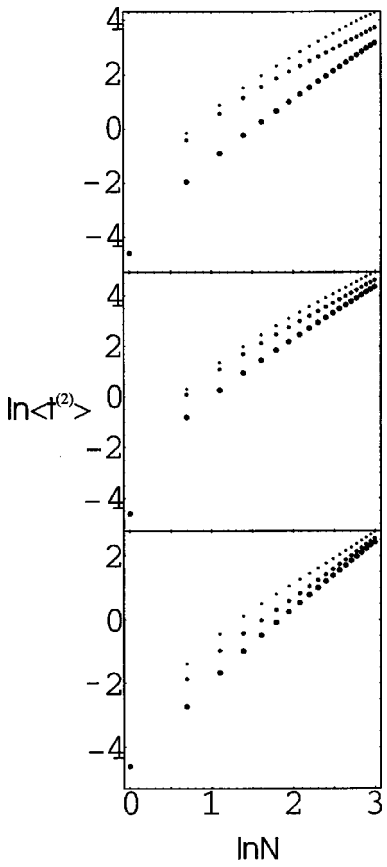


FIG. 9. Log-log plots of $\langle t^{(2)}\rangle$ vs $N$ for models $M1-M3$ (top panel), $M4-M6$ (middle panel), and $M7-M9$ (bottom panel). Size of circles increases with bath jump rates as in Fig. 5.

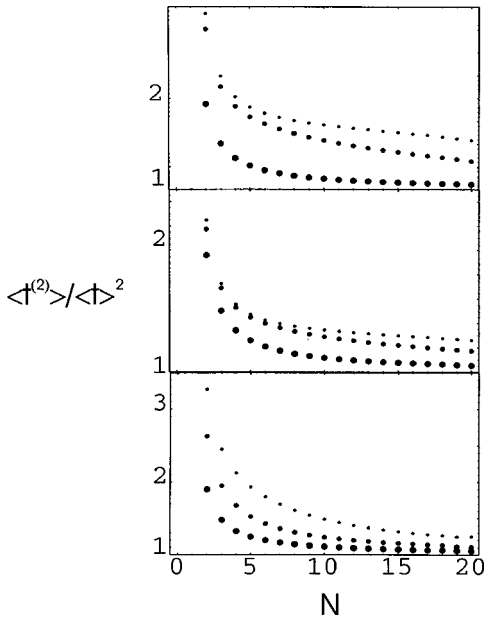


FIG. 10. Plots of the dimensionless ratio $\langle t^{(2)}\rangle/\langle t\rangle^2$ vs $N$ for models $M1-M3$ (top panel), $M4-M6$ (middle panel), and $M7-M9$ (bottom panel). Size of circles increases with bath jump rates as in Fig. 5.

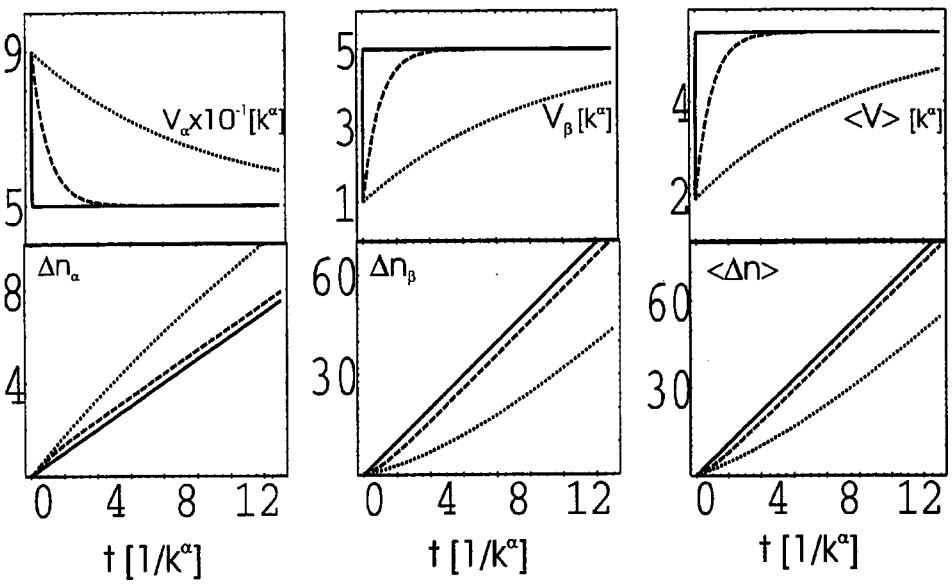


FIG. 11. Top: $V_\alpha(t)$ (left panels), $V_\beta(t)$ (middle panels), and $\langle V(t)\rangle$ (right panels) vs $t$ for models $M10$ (dotted lines), $M11$ (dashed lines), and $M12$ (solid lines). Bottom: $\Delta n_\alpha(t)$ (left panels), $\Delta n_\beta(t)$ (middle panels), and $\langle \Delta n(t)\rangle$ (right panels) vs $t$ for models $M10$ (dotted lines), $M11$ (dashed lines), and $M12$ (solid lines). Initial populations of states $\alpha$ and $\beta$ of the donor are $P_\alpha(0)=0.95$ and $P_\beta(0)=0.05$.

tion of $r$ with $N$ demonstrates that higher moments of mean quenching time provide additional information to that contained in the MQT.

## V. DISTRIBUTIONS OF COORDINATE, VELOCITY, AND DIFFUSION COEFFICIENT

We now examine the scaling behavior of excitation coordinate $n$, velocity $V$, and diffusion coefficient $D$ in the limit when $N\to\infty$. The velocity distribution is defined by

$$V_\mu \equiv \frac{d}{dt} n_\mu(t), \quad \mu=\alpha,\beta, \tag{35}$$

and the average velocity function is

$$\langle V(t)\rangle = \frac{d}{dt}\langle n(t)\rangle = V_\alpha + V_\beta. \tag{36}$$

The distribution of excitation coordinate $n_\mu(t)$ and the average coordinate $\langle n(t)\rangle$ can be obtained by integrating $V_\alpha(t)$, $V_\beta(t)$, and $\langle V(t)\rangle$ with initial condition $n(0)=1$.

It follows from Eq. (1) that

$$\frac{d}{dt}\langle n(t)\rangle = \sum_{n=0}^{\infty} n \frac{d}{dt}[P_\alpha^{[n]}(t)+P_\beta^{[n]}(t)]$$

$$= k^\alpha \sum_{n=0}^{\infty} P_\alpha^{[n]}(t) + k^\beta \sum_{n=0}^{\infty} P_\beta^{[n]}(t), \tag{37}$$

where the total populations $P_\alpha \equiv \Sigma_{n=0}^{\infty} P_\alpha^{[n]}$ and $P_\beta \equiv \Sigma_{n=0}^{\infty} P_\beta^{[n]}$ of channel $\alpha$ and $\beta$ obey the system of coupled differential equations

$$\frac{d}{dt}\begin{pmatrix} P_\alpha(t) \\ P_\beta(t)\end{pmatrix} = \begin{pmatrix} -R_{\beta\alpha} & R_{\alpha\beta} \\ R_{\beta\alpha} & -R_{\alpha\beta}\end{pmatrix}\begin{pmatrix} P_\alpha(t) \\ P_\beta(t)\end{pmatrix}, \tag{38}$$

Eqs. (38) can be readily solved to give

$$\begin{pmatrix} P_\alpha(t) \\ P_\beta(t)\end{pmatrix} = \begin{pmatrix} g_{\alpha\alpha}(t) & g_{\alpha\beta}(t) \\ g_{\beta\alpha}(t) & g_{\beta\beta}(t)\end{pmatrix}\begin{pmatrix} P_\alpha(0) \\ P_\beta(0)\end{pmatrix}, \tag{39}$$

where the Green functions $g_{\alpha\alpha}(t)$ and $g_{\alpha\beta}(t)$ are given by $g_{\alpha\alpha}(t)=R^{-1}(R_{\alpha\beta}+R_{\beta\alpha}e^{-Rt})$ and $g_{\alpha\beta}(t)=R^{-1}(R_{\alpha\beta}-R_{\beta\alpha}e^{-Rt})$, respectively, and $g_{\beta\alpha}(t)$ and $g_{\beta\beta}(t)$ are obtained by interchanging indices $\alpha\leftrightarrow\beta$. These functions describe propagation of the total occupation probability from channel $\mu$ to $\nu$ $(\mu,\nu=\alpha,\beta)$ subject to initial condition $P_\alpha(0)\equiv\Sigma_{n=0}^{\infty}P_\alpha^{[n]}(0)$, $P_\beta(0)\equiv\Sigma_{n=0}^{\infty}P_\beta^{[n]}(0)$, and $P_\alpha(0)+P_\beta(0)=1$.

Using Eqs. (39), we obtain for the average velocity function

$$\langle V(t)\rangle = k^\alpha w_{eq}^\alpha + k^\beta w_{eq}^\beta + \frac{\Delta k}{R}[R_{\beta\alpha}P_\alpha(0) - R_{\alpha\beta}P_\beta(0)]e^{-Rt}, \tag{40}$$

where $\Delta k \equiv k^\alpha - k^\beta$ is the magnitude of disorder. It follows from Eq. (40) that $\langle V(t)\rangle$ starts off from its value $k^\alpha P_\alpha(0)+k^\beta P_\beta(0)$ at time $t=0$ and asymptotically approaches the limit

$$\langle V\rangle = \lim_{t\to\infty}\langle V(t)\rangle = k^\alpha w_{eq}^\alpha + k^\beta w_{eq}^\beta, \tag{41}$$

where $V_\alpha = k^\alpha w_{eq}^\alpha$ and $V_\beta = k^\beta w_{eq}^\beta$ is the distribution of excitation velocity. The transient part [second term in Eq. (40)] decays on the time scale of bath relaxation $R^{-1}$. Thus, dynamic disorder self-averages when $t \gg R^{-1}$.

In Fig. 11 (upper panels), we plot the distribution of velocity

$$V_\alpha(t) = k^\alpha w_{eq}^\alpha + R^{-1}k^\alpha R_{\beta\alpha}P_\alpha(0)\exp[-Rt], \tag{42}$$
$$V_\beta(t) = k^\beta w_{eq}^\alpha - R^{-1}k^\beta R_{\alpha\beta}P_\beta(0)\exp[-Rt],$$

and $\langle V(t)\rangle$ for models $M10$, $M11$, and $M12$ with $\kappa \gg 1$, $\kappa \sim 1$, and $\kappa \ll 1$, respectively (see Table I). Note that since in our calculation $\Delta k<0$, $V_\beta(t)$ grows at the expense of $V_\alpha(t)$. All three quantities, $V_\alpha(t)$, $V_\beta(t)$, and $\langle V(t)\rangle$, approach their respective asymptotic limits, $V_\alpha$, $V_\beta$, and $\langle V\rangle$, as $\kappa \to 0$.

The distribution of the $p$th moment ($p=1,2,\ldots$) of excitation coordinate is defined by

$$n_\mu^p \equiv \sum_{n=0}^{\infty} n^p P_\mu^{[n]}, \quad \mu = \alpha, \beta, \tag{43}$$

where $P_\alpha^{[n]}(t)$ and $P_\beta^{[n]}(t)$ are populations of states $|n\alpha\rangle$ and $|n\alpha\rangle$. The average coordinate is given by

$$\langle n^p(t)\rangle \equiv \sum_{n=0}^{\infty} n^p P^{[n]}(t) = n_\alpha^p + n_\beta^p. \tag{44}$$

The distribution of coordinates $n_\alpha(t)$, $n_\beta(t)$ and the average coordinate $\langle n(t)\rangle$ can now be obtained by integrating $V_\alpha(t)$, $V_\beta(t)$, and $\langle V(t)\rangle$ subject to initial condition $n(t=0)=n_0$. For $\langle n(t)\rangle$, we obtain

$$\langle n(t)\rangle = n_0 + (k^\alpha w_{eq}^\alpha + k^\beta w_{eq}^\beta)t + \frac{\Delta k}{R^2}[R_{\beta\alpha}P_\alpha(0) - R_{\alpha\beta}P_\beta(0)](1-e^{-Rt}). \tag{45}$$

The distribution of displacement given by

$$\Delta n_\alpha(t) \equiv n_\alpha(t) - n_{\alpha 0} = k^\alpha w_{eq}^\alpha t + R^{-2} k^\alpha R_{\beta\alpha} P_\alpha(0) \times (1 - \exp[-Rt]), \tag{46}$$

$$\Delta n_\beta(t) \equiv n_\beta(t) - n_{\beta 0} = k^\beta w_{eq}^\beta t - R^{-2} k^\beta R_{\alpha\beta} P_\beta(0) \times (1 - \exp[-Rt]),$$

and the average displacement $\langle \Delta n(t)\rangle \equiv \langle n(t)\rangle - n_0$ for models $M10-M12$ is plotted in Fig. 11 (lower panels). Again, we see that all three quantities, $\Delta n_\alpha(t)$, $\Delta n_\beta(t)$, and $\langle \Delta n(t)\rangle$ approach linear scaling, $\Delta n_\alpha(t) \sim k^\alpha w_{eq}^\alpha t$, $\Delta n_\beta(t) \sim k^\beta w_{eq}^\beta t$, and $\langle \Delta n(t)\rangle \sim (k^\alpha w_{eq}^\alpha + k^\beta w_{eq}^\beta)t$ after the dynamic disorder self-averages.

We next examine the distribution of higher moments of excitation coordinate $n_\alpha^p(t)$, $n_\beta^p(t)$ and higher moments of the average excitation coordinate $\langle n^p(t)\rangle$ $(p>1)$. For $\langle n^p(t)\rangle$, we obtain

$$\begin{aligned}\frac{d\langle n^p(t)\rangle}{dt} &= k^\alpha \sum_{n=0}^{\infty} [(n+1)^p - n^p] P_\alpha^{[n]}(t) + k^\beta \sum_{n=0}^{\infty} [(n+1)^p - n^p] P_\beta^{[n]}(t) \\ &= k^\alpha \sum_{l=1}^{p} C_p^l \sum_{n=0}^{\infty} n^{p-l} P_\alpha^{[n]}(t) + k^\beta \sum_{l=1}^{p} C_p^l \sum_{n=0}^{\infty} n^{p-l} P_\beta^{[n]}(t) + \sum_{l=1}^{p-1} C_p^l [k^\alpha n_\alpha^{p-1}(t) + k^\beta n_\beta^{p-1}(t)] + k^\alpha \sum_{n=0}^{\infty} P_\alpha^{[n]}(t) + k^\beta \sum_{n=0}^{\infty} P_\beta^{[n]}(t),\end{aligned} \tag{47}$$

where $C_p^l = p!/[l!(p-l)!]$. Equation (47) implies that the distribution of $p$th moments of excitation coordinate can be computed recursively from the corresponding distribution of moments of order $p-1$.

The distribution of second moments $n_\alpha^2(t)$, $n_\beta^2(t)$ and the average second moment $\langle n^2(t)\rangle$ are obtained by setting $p=2$ in Eq. (47), i.e.,

$$\frac{d\langle n^2(t)\rangle}{dt} = \frac{d}{dt}[n_\alpha^2(t) + n_\beta^2(t)] = k^\alpha[n_\alpha(t) + P_\alpha(t)] + k^\beta[n_\beta(t) + P_\beta(t)]. \tag{48}$$

Inserting $n_\alpha(t)$, $n_\alpha(t)$, $P_\alpha(t)$, and $P_\beta(t)$ into Eq. (48) and integrating Eq. (48), we obtain the distribution of second moments,

$$\begin{aligned} n_\alpha^2(t) &= n_{\alpha 0}^2 + \left[ n_{\alpha 0} k^\alpha + k^\alpha w_{eq}^\alpha + \frac{[k^\alpha]^2}{R^2}[R_{\beta\alpha}P_\alpha(0) - R_{\alpha\beta}P_\beta(0)] \right] t + \frac{1}{2}[k_\alpha]^2 w_{eq}^\alpha t^2 + \left( \frac{k^\alpha}{R^2} - \frac{[k^\alpha]^2}{R^3} \right) \\ &\quad \times [R_{\beta\alpha}P_\alpha(0) - R_{\alpha\beta}P_\beta(0)](1-e^{-Rt}), \\ n_\beta^2(t) &= n_{\beta 0}^2 + \left[ n_{\beta 0} k^\beta + k^\beta w_{eq}^\beta - \frac{[k^\beta]^2}{R^2}[R_{\beta\alpha}P_\alpha(0) - R_{\alpha\beta}P_\beta(0)] \right] t + \frac{1}{2}[k^\beta]^2 w_{eq}^\beta t^2 - \left( \frac{k^\beta}{R^2} - \frac{[k^\beta]^2}{R^3} \right) \\ &\quad \times [R_{\beta\alpha}P_\alpha(0) - R_{\alpha\beta}P_\beta(0)](1-e^{-Rt}), \end{aligned} \tag{49}$$

where $n_{\alpha 0}^2 = n_\alpha^2(0)$, $n_{\beta 0}^2 = n_\beta^2(0)$ are initial conditions $(n_{\alpha 0}^2 + n_{\beta 0}^2 = 1)$ and the average second moment is $\langle n^2(t)\rangle = n_\alpha^2(t) + n_\beta^2(t)$.

Plots of $\Delta n_\alpha^2(t)$, $\Delta n_\beta^2(t)$, and $\langle \Delta n^2(t)\rangle$ for models $M10-M12$ are presented in Fig. 12 (upper panels). The amplitude of $\Delta n_\alpha^2$ for a slow channel ($\Delta n_\beta^2$ for a fast channel) increases (decreases) with bath relaxation time scale. As follows from Eqs. (49) and seen in Fig. 12, all three quantities $\Delta n_\alpha^2(t)$, $\Delta n_\beta^2(t)$, and $\langle \Delta n^2(t)\rangle$ scale linearly with time for short times and quadratically for long times. In the intermediate time regime ($Rt \sim 1$), the dynamic disorder [terms containing factor $1-\exp[-Rt]$ in Eqs. (49)] gives nonvanishing contribution.

We have also computed the distribution of diffusion function $D_\alpha(t)$ and $D_\beta(t)$ defined by

$$\begin{pmatrix} D_\alpha(t) \\ D_\beta(t) \end{pmatrix} = \frac{1}{2}\frac{d}{dt}\left[ \begin{pmatrix} n_\alpha^2(t) \\ n_\beta^2(t) \end{pmatrix} - \begin{pmatrix} n_\alpha(t)^2 \\ n_\beta(t)^2 \end{pmatrix} \right], \tag{50}$$

and the average diffusion function $\langle D(t)\rangle$,

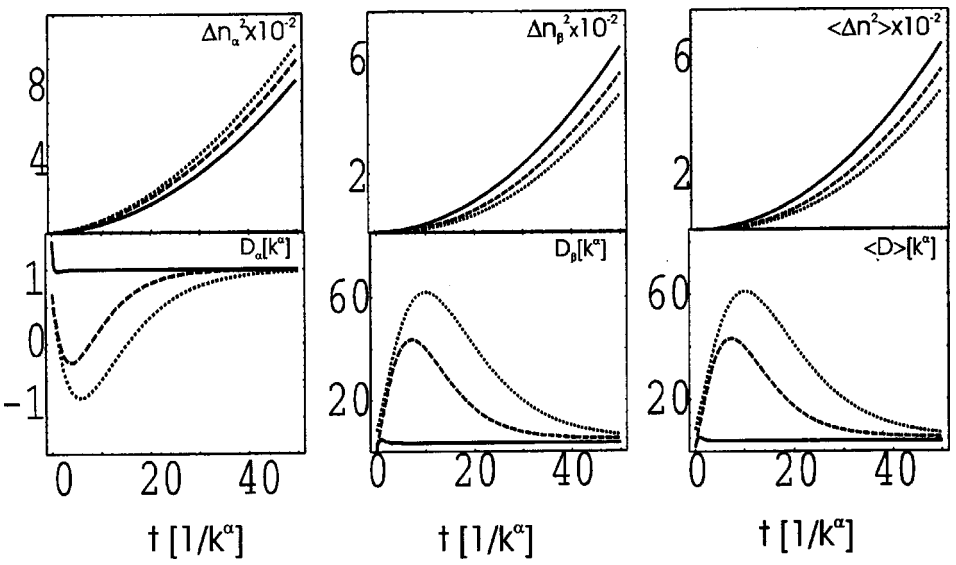


FIG. 12. Top: $\Delta n_\alpha^2(t)$ (left panels), $\Delta n_\beta^2(t)$ (middle panels), and $\langle \Delta n^2(t) \rangle$ (right panels) vs $t$ for models $M10$ (dotted lines), $M11$ (dashed lines), and $M12$ (solid lines). Bottom: $D_\alpha(t)$ (left panels), $D_\beta(t)$ (middle panels), and $\langle D(t) \rangle$ (right panels) vs $t$ for models $M10$ (dotted lines), $M11$ (dashed lines), and $M12$ (solid lines). $P_\alpha(0)$ and $P_\beta(0)$ are as in Fig. 11.

$$\langle D(t) \rangle = \frac{1}{2} \frac{d}{dt} [\langle n^2(t) \rangle - \langle n(t) \rangle^2]. \tag{51}$$

Expressions for $D_\alpha(t)$, $D_\beta(t)$, and $\langle D(t) \rangle$ are too lengthy and will not be presented.

In Fig. 12 (lower panels), we display $D_\alpha(t)$, $D_\beta(t)$, and $\langle D(t) \rangle$ for models $M10-M12$. Note drastic difference in the amplitude of diffusion coefficients for slow and fast channels. We see that only after the dynamic disorder averages out (i.e., for $N$ such that $N\kappa \ll 1$) do $D_\alpha(t)$, $D_\beta(t)$, and $\langle D(t) \rangle$ approach their limiting distribution given by diffusion coefficients $D_{\alpha,\beta} = \lim_{t\to\infty} D_{\alpha,\beta}(t)$ and the average diffusion coefficient $\langle D \rangle = \lim_{t\to\infty} \langle D(t) \rangle$. A slow channel (fast channel) approaches its asymptotics $D_\alpha$ ($D_\beta$) from below (above), which reflects conservation of the total probability in channels $\alpha$ and $\beta$.

Note that before the disorder self-averages, $D_\alpha$ may become negative, implying the absence of excitation transfer in channel $\alpha$ and funneling of the distribution from channel $\alpha$ to channel $\beta$ at short times. However, as the disorder self-averages at longer times, $D_\alpha$ becomes positive.

## VI. CONCLUSIONS

In this paper, we studied the effects of a fluctuating environment on transport, modeled by a directed one-dimensional walk. We consider a walker created at time $t = 0$ on the first site of the chain and destroyed at some later time on a terminal site $N$. The fluctuating environment is described by stochastic jumps between two states of the bath. In this stochastic model, transport is affected by the bath dynamics but the bath is not affected by transport.

We studied the dynamics when the waiting time for a walker to hop to the next nearest neighbor are exponentially distributed in a regime when both transport and bath fluctuations occur on a comparable time scale assuming the same transfer rates for all sites. The present analysis could be extended to include both static and dynamic disorder as well as backward transitions.

Examination of the probability distribution of quenching at the terminal site shows that when hopping rates associated with bath states are notably different, bath state dependent quenching probabilities develop interesting dynamical pattern (i.e., anomalously long quenching time tails for a slow channel and peaks at short times for a fast channel) with the average quenching probability exhibiting multiply peaked long quenching tails. This implies that in the presence of fluctuating environment when $R$ is comparable with the MQT, random walk becomes a non-Markovian process once the bath is eliminated. When bath jumps are fast compared with transport time, quenching probabilities and the average probability are identically distributed. In this limit, we merely see the average channel since self-averaging sets in on the bath time scale almost immediately.

These findings motivated our study of scaling of the entire distribution of quenching time and the MQT with $N$. In the absence of dynamic disorder when the waiting times are exponentially distributed, the average posing time for a directed walker is inversely proportional to the hopping rate and the MQT is linear in $N$. However, with disorder partial first moments of quenching time and the MQT $\langle t \rangle$ notably deviate from linear scaling. We found that $\langle t \rangle \sim N^{1+\gamma}$ where the fractional part of the exponent $\gamma$ scales with $N$ as $1/\ln N$ and is inversely proportional to the bath jump time scale. Therefore, as the dynamic disorder self-averages, deviations of $\langle t \rangle$ from linear scaling gradually disappear for a longer walk or faster bath jumps. Only when $N\kappa \ll 1$, does $\langle t \rangle$ approaches asymptotically linear scaling, $\langle t \rangle \sim N$. The existence of finite fractional counterpart $\gamma$ is directly related to non-Markovian long tails of the distribution of quenching probabilities and is a result of the memory of the random walker to its initial state.

We have further examined partial second moments of quenching time and the average second moment $\langle t^{(2)} \rangle$. Similar to the behavior of $\langle t \rangle$, we found deviations of $\langle t^{(2)} \rangle$ from quadratic dependence and that $\langle t^{(2)} \rangle \sim N^2$ only after the dynamic disorder is self-averaged. In view of the interesting types of dynamic behavior for $\langle t \rangle$ and $\langle t^2 \rangle$, we examined the

inverse problem, namely, how the length of a directed walk scales with time (i.e., $\langle n\rangle$ and $\langle n^2\rangle$ as functions of $t$) in the limit when $N$ is infinite. We computed the distribution of displacements, average displacement, the distribution of displacement second moments, and the average second moment of displacement. We have shown that the distribution of higher ($p$th) moments of coordinate can be computed from the distribution of moments of lower order $(p-1)$.

Similar to $\langle t(N)\rangle$ and $\langle t^2(N)\rangle$, $\langle \Delta n(t)\rangle$, and $\langle \Delta n^2(t)\rangle$ exhibit interesting scaling behavior with time: $\langle \Delta n\rangle$ scales linearly with $t$ only after the transient part reflecting dynamic disorder decays to zero on the time scale $R^{-1}$; $\langle \Delta n^2\rangle$ scales linearly with time for times shorter than $R^{-1}$ and quadratically for times longer than $R^{-1}$ with the cross over facilitated by the transient term (decaying exponentially on the time scale $R^{-1}$) coming from dynamic disorder. We have also computed the distributions of velocity and diffusion coefficient, and the average velocity and diffusion coefficient and found that only after the dynamic disorder self-averages, do distributions of velocity and diffusion coefficients approach their limiting constant values.


## ACKNOWLEDGMENT

The support of the Office of Basic Energy Science of the Department of Energy, Grant No. DE-FG02-01ER15155 is gratefully acknowledged.


## APPENDIX: RECURSIVE CALCULATION OF THE GREEN FUNCTIONS

The Green functions $\tilde{G}^{[n+1]}_{\alpha\alpha}(z)$ and $\tilde{G}^{[n+1]}_{\alpha\beta}(z)$ for the $(n+1)$-site transfer problem can be obtained from Green functions $\tilde{G}^{[n]}_{\alpha\alpha}(z)$ and $\tilde{G}^{[n]}_{\alpha\beta}(z)$ for the $n$-site problem by the following matrix transformation:

$$\begin{pmatrix} \tilde{G}^{[n+1]}_{\alpha\alpha}(z) \\ \tilde{G}^{[n+1]}_{\alpha\beta}(z) \end{pmatrix} = \tilde{\mathbf{A}}_n(z) \begin{pmatrix} \tilde{G}^{[n]}_{\alpha\alpha}(z) \\ \tilde{G}^{[n]}_{\alpha\beta}(z) \end{pmatrix}, \tag{A1}$$

where the generating matrix $\tilde{\mathbf{A}}_n(z)$ is defined by

$$\tilde{\mathbf{A}}_n(z) \equiv \frac{1}{\det[\tilde{\mathbf{P}}^{[n]}(z)+\mathbf{R}]} [\tilde{\mathbf{P}}^{[n]}(z)+\mathbf{R}]\tilde{\mathbf{\Phi}}^{(n)}(z), \tag{A2}$$

where matrix $\tilde{\mathbf{P}}^{[n]}(z)$ of excitation propagators is given by

$$\mathbf{P}^{[n]}(z) = \begin{pmatrix} z+\tilde{\phi}^{\beta}_n(z) & 0 \\ 0 & z+\tilde{\phi}^{\alpha}_n(z) \end{pmatrix}, \tag{A3}$$

matrix $\tilde{\mathbf{\Phi}}^{(n)}(z)$ is obtained by Laplace transformation of entrees of matrix $\mathbf{\Phi}^{(n)}(t)$ given by Eq. (4), and matrix $\mathbf{R}$ is given by Eq. (6). Similarly, Green functions $\tilde{G}^{[n+1]}_{\beta\alpha}(z)$ and $\tilde{G}^{[n+1]}_{\beta\beta}(z)$ can be obtained from $\tilde{G}^{[n]}_{\beta\alpha}(z)$ and $\tilde{G}^{[n]}_{\beta\beta}(z)$ by the transformation in which we have interchanged $\tilde{\phi}^{\alpha}_n(z) \leftrightarrow \tilde{\phi}^{\beta}_n(z)$ and $R_{\alpha\beta} \leftrightarrow R_{\beta\alpha}$.

The matrix transformation $\tilde{\mathbf{A}}_n(z)$ in Eq. (A1) allows to derive a recursion relation between the $n$-site and $(n+1)$-site problem. Alternatively, the matrix transformation $[\tilde{\mathbf{A}}_n(z)]^{-1}$ inverse to $\tilde{\mathbf{A}}_n(z)$, reduces the $(n+1)$-site problem into the $n$-site problem. Therefore, applying transformation $\tilde{\mathbf{A}}_n(z)$ to Green functions $\tilde{G}^{[1]}_{\alpha\alpha}(z)$ and $\tilde{G}^{[1]}_{\alpha\beta}(z)$ for 1-site problem $N-1$ times, we obtain Green functions for $N$-site problem, i.e.,

$$\begin{pmatrix} \tilde{G}^{[N]}_{\alpha\alpha}(z) \\ \tilde{G}^{[N]}_{\alpha\beta}(z) \end{pmatrix} = \tilde{\mathbf{A}}^{N-1}_n(z) \begin{pmatrix} \tilde{G}^{[1]}_{\alpha\alpha}(z) \\ \tilde{G}^{[1]}_{\alpha\beta}(z) \end{pmatrix}. \tag{A4}$$

Although Eq. (A4) has a simple form, it is not practical for computations with large $N$. To make it more useful, we solve the eigenvalue problem for $\tilde{\mathbf{A}}_n(z)$, i.e.,

$$\tilde{\mathbf{A}}_n(z) \begin{pmatrix} \tilde{G}^{[1]}_{\alpha\alpha}(z) \\ \tilde{G}^{[1]}_{\alpha\beta}(z) \end{pmatrix} = \tilde{\mathbf{a}}_n(z) \begin{pmatrix} \tilde{G}^{[1]}_{\alpha\alpha}(z) \\ \tilde{G}^{[1]}_{\alpha\beta}(z) \end{pmatrix}, \tag{A5}$$

where $\tilde{\mathbf{a}}_n(z)$ is the matrix of eigenvalues $\tilde{\lambda}_{n,1}(z)$ and $\tilde{\lambda}_{n,2}(z)$ of $\mathbf{A}_n(z)$.

In the absence of static disorder, $\tilde{\lambda}_{1,1}(z)=\tilde{\lambda}_{2,1}(z)=\cdots=\tilde{\lambda}_1(z)$ and $\tilde{\lambda}_{1,2}(z)=\tilde{\lambda}_{2,2}(z)=\cdots=\tilde{\lambda}_2(z)$, and solving the eigenvalue problem (A5) $N-1$ times, we finally obtain Eq. (13).

Equation (13) sums the $2^{N-1}$ diagrams in calculation of $\tilde{G}^{[N]}_{\alpha\alpha}$ and $\tilde{G}^{[N]}_{\alpha\beta}$ and the result is $\Pi^{N-1}_{i=2}\tilde{\lambda}_{i,1}\tilde{G}^{[1]}_{\alpha\alpha}(z)$ and $\Pi^{N-1}_{i=2}\tilde{\lambda}_{i,2}\tilde{G}^{[1]}_{\alpha\beta}(z)$, respectively. Note that the eigenvalues $\tilde{\lambda}_{i,1}$ and $\tilde{\lambda}_{i,2}$ must remain invariant with respect to the interchange $\alpha \leftrightarrow \beta$, and for the other pair of Green functions $\tilde{G}^{[N]}_{\beta\alpha}$ and $\tilde{G}^{[N]}_{\beta\beta}$, we obtain

$$\begin{pmatrix} \tilde{G}^{[N]}_{\beta\alpha}(z) \\ \tilde{G}^{[N]}_{\beta\beta}(z) \end{pmatrix} = \begin{pmatrix} \tilde{\lambda}^{N-1}_1(z) & 0 \\ 0 & \tilde{\lambda}^{N-1}_2(z) \end{pmatrix} \begin{pmatrix} \tilde{G}^{[1]}_{\beta\alpha}(z) \\ \tilde{G}^{[1]}_{\beta\beta}(z) \end{pmatrix}. \tag{A6}$$

The bath state dependent $\alpha\alpha$ and $\alpha\beta$ elements of Green function matrix for $N$-site problem depend on $\alpha\alpha$ and $\alpha\beta$ elements for the problem involving a single site. In this "two-eigenchannel" picture, excitation pathways from state of the bath $|1\mu\rangle$ to state $|N\nu\rangle$ ($\mu$, $\nu=\alpha$, $\beta$) are decoupled.


[1] V.M. Kenkre, in *Exciton Dynamics in Molecular Crystals and Aggregates*, edited by G. Hohler (Springer, Berlin, 1982).

[2] S. W. Haan and R. Zwanzig, J. Chem. Phys. **68**, 1879 (1978).

[3] T. Odagaki and M. Lax, Phys. Rev. B **25**, 2307 (1982); **26**, 6480 (1983).

[4] R.F. Loring, M. Sparpaglione, and S. Mukamel, J. Chem. Phys. **86**, 2249 (1987).

[5] B. Derrida, J. Stat. Phys. **31**, 433 (1983).

[6] M.F. Shlesinger, J. Stat. Phys. **10**, 421 (1973).

[7] E.W. Montroll and H. Scher, J. Stat. Phys. **9**, 101 (1973); Phys. Rev. B **12**, 2455 (1975); H. Scher and M. Lax, *ibid.* **7**, 4491 (1973); **7**, 4502 (1973).

[8] S. Alexander, J. Bernasconi, W.R. Schneider, and R. Orbach, Rev. Mod. Phys. **53**, 175 (1981).
[9] S. Alexander, J. Bernasconi, W.R. Schneider, and R. Orbach, in *Springer Series in Solid-State Sciences*, edited by J. Bernasconi and T. Schneider (Springer, Berlin, 1981), Vol. 23, p. 277.
[10] T. Ha, Th. Enderle, D.F. Ogletree, D.S. Chemla, P.R. Selvin, and S. Weiss, Proc. Natl. Acad. Sci. U.S.A. **93**, 6264 (1996).
[11] C. Eggeling, J.R. Fries, L. Brand, R. Guenter, and C.A.M. Seidel, Proc. Natl. Acad. Sci. U.S.A. **95**, 1556 (1998); J. Tellinghuisen, P.M. Goodwin, W.P. Ambrose, J.C. Martin, and P.M. Keller, Anal. Chem. **66**, 64 (1994).
[12] V. Barsegov and S. Mukamel, J. Chem. Phys. **116**, 9802 (2002).
[13] F.L.H. Brown, D.M. Leitner, J.A. McCammon, and K. Wilson, Biophys. J. **78**, 2257 (2000); **78**, 125 (2000); F.L.H. Brown, *ibid.* **84**, 842 (2003); M.J. Saxton, *ibid.* **55**, 21 (1989); **57**, 1167 (1990); **69**, 389 (1995).
[14] M. Edidin, S.C. Kuo, and M.P. Sheetz, Science **254**, 1379 (1991).
[15] D.H. Boal, Biophys. J. **67**, 521 (1994); D.H. Boal and S.K. Boey, *ibid.* **69**, 372 (1995).
[16] M.A. Ratner, Nature (London) **397**, 480 (1999).
[17] Y.A. Berlin, A.L. Burin, and M.A. Ratner, J. Phys. Chem. A **104**, 443 (2000); M. Olson, Y. Mao, T. Windus, M. Kemp, M.A. Ratner, N. Leon, and V. Mujica, J. Phys. Chem. B **102**, 941 (1999).
[18] A. Tikhonov, R.D. Coalson, and Y. Dahnovsky, J. Chem. Phys. **116**, 10 909 (2002); **117**, 567 (2002).
[19] V. Barsegov, V. Chernyak, and S. Mukamel, J. Chem. Phys. **116**, 4240 (2002).
[20] D.J. Bicout and A. Szabo, J. Chem. Phys. **108**, 5491 (1998).
[21] R. Zwanzig, J. Chem. Phys. **97**, 3587 (1992).
[22] N. Eisenberg and J. Klafter, J. Chem. Phys. **104**, 6796 (1996); Physica A **249**, 424 (1998).
[23] N. Eisenberg and J. Klafter, Chem. Phys. Lett. **243**, 9 (1995); **287**, 442 (1998).
[24] P. Graf, A. Nitzan, M.G. Kurnikova, and R.D. Coalson, J. Phys. Chem. B **104**, 12 324 (2000); Biophys. J. **76**, 642 (1999).
[25] J. Chuang, Y. Kantor, and M. Kardar, Phys. Rev. E **65**, 011802 (2001).
[26] S.E. Henrickson, M. Misakian, B. Robertson, and J. Kasianowicz, Phys. Rev. Lett. **85**, 3057 (2000).
[27] M. Muthukumar, J. Chem. Phys. **111**, 10 371 (1999); Phys. Rev. Lett. **86**, 3188 (2001).
[28] P.G. de Gennes, Physica A **274**, 1 (1999).
[29] D.K. Lubensky and D.R. Nelson, Biophys. J. **77**, 1824 (1999).
[30] R.M. Dickson, D.J. Norris, Y.-L. Tzeng, and W.E. Moerner, Science **274**, 966 (1996).
[31] X.-H. Xu and E.S. Young, Science **275**, 1066 (1997).
[32] T. Ha, J. Glass, T. Enderle, D.S. Chemla, and S. Weiss, Phys. Rev. Lett. **80**, 2093 (1998).
[33] H.P. Lu and X.S. Xie, Nature (London) **385**, 143 (1997).
[34] S. Wennmaim, L. Edman, and R. Rigler, Proc. Natl. Acad. Sci. U.S.A. **94**, 10 641 (1997).
[35] D.A. Vanden Bout, W.-T. Yip, D. Hu, D.-K. Fu, T.M. Swager, and P. Barbara, Science **277**, 1074 (1997).
[36] V. Barsegov and S. Mukamel (unpublished).
[37] H.P. Lu, L. Xun, and X.S. Xie, Science **282**, 187 (1998); G.K. Schenter, H.P. Lu, and X.S. Xie, J. Phys. Chem. A **103**, 10477 (1999).
[38] J.-P. Bouchaud and M. Mezard, J. Phys. A **30**, 7997 (1997); M. Mezard, G. Parisi, and M.A. Virasoro, *Spin Glass Theory and Beyond* (World Scientific, Singapore, 1987).
[39] J.-P. Bouchaud, L.F. Cugliandolo, J. Kurchan, and M. Mezard, in *Spin Glasses and Random Fields*, edited by A.P. Young (World Scientific, Singapore, 1998), pp. 2613–2626.
[40] S. Raychaudhuri, Y. Shapir, V. Chernyak, and S. Mukamel, Phys. Rev. Lett. **85**, 282 (2000); S. Raychaudhuri, Y. Shapir, and S. Mukamel, Phys. Rev. E **65**, 021803 (2002).
[41] D. Keller and C. Bustamante, Biophys. J. **78**, 451 (2000); C. Bustamante, D. Keller, and G. Oster, Acc. Chem. Res. **34**, 412 (2001).
[42] P.W. Andersen, J. Phys. Soc. Jpn. **9**, 316 (1954); P.W. Andersen, B.I. Halperin, and C.M. Varma, Philos. Mag. **25**, 1 (1971).
[43] R. Kubo, J. Phys. Soc. Jpn. **6**, 935 (1954); Adv. Chem. Phys. **15**, 101 (1969); in *Fluctuations Relaxation and Resonance in Magnetic Systems*, edited by D. ter Haar (Plenum, New York, 1962).
[44] V. Chernyak, M. Schulz, and S. Mukamel, J. Chem. Phys. **111**, 7416 (1999).
[45] P.D. Reilly and J.L. Skinner, Phys. Rev. Lett. **71**, 4257 (1993); J. Chem. Phys. **101**, 965 (1994).
[46] E. Geva and J.L. Skinner, J. Phys. Chem. B **101**, 8920 (1997).
[47] E. Barkai, Y.-J. Jung, and R. Silbey, Phys. Rev. Lett. **87**, 207403 (2001).
[48] M.P. Sheetz, M. Schindler, and D.E. Koppel, Nature (London) **285**, 510 (1980).
[49] J.-P. Bouchaud and A. Georges, Phys. Rep. **195**, 127 (1990).
[50] J. Machta, Phys. Rev. B **24**, 5260 (1981).
[51] H. van Beijeren, Rev. Mod. Phys. **54**, 195 (1982).
[52] B.D. Hughes, *Random Walks and Random Environment* (Clarendon, Oxford, 1995), Vols. 1 and 2.